Structural basis of FFAT Motif-mediated ER targeting

Stephen E. Kaiser, Jason H. Brickner[1], Amy R. Reilein, Tim D. Fenn, Peter Walter[1], Axel T. Brunger[2,3]

Department of Molecular and Cellular Physiology, Stanford University, Stanford, California, USA

[1]Howard Hughes Medical Institute and the Department of Biochemistry and Biophysics, University of California, San Francisco, California, USA

[2]Howard Hughes Medical Institute and Departments of Molecular and Cellular Physiology, Neurology and Neurological Sciences, and Stanford Synchrotron Radiation Laboratory, Stanford University, James H. Clark Center E300-C, 318 Campus Drive, Stanford, California, USA 94305-5432.

[3]Corresponding author
E-mail: brunger@stanford.edu

Running Title: VAP-FFAT Complex Structure

Character Count: 49,935

The FFAT motif is a targeting signal responsible for localizing a number of proteins to the cytosolic surface of the endoplasmic reticulum (ER) and to the nuclear membrane. FFAT motifs bind to the highly conserved protein VAP-33, which is tethered to the cytoplasmic face of the ER by a C-terminal transmembrane domain. We find that VAP proteins bind FFAT motifs through a highly conserved N-terminal Major Sperm Protein (MSP) homology domain with 1:1 stoichiometry. We have solved crystal structures of the rat VAP-A MSP homology domain alone and in complex with an FFAT motif. The co-crystal structure was used to design a VAP mutant that disrupts rat and yeast VAP-FFAT interactions *in vitro.* The FFAT binding-defective mutant also blocked function of the VAP homologue Scs2p in yeast. Finally, overexpression of the FFAT binding-defective VAP in COS7 cells dramatically altered ER morphology. Our data establish the structural basis of FFAT-mediated ER targeting and suggest that FFAT targeted proteins play an important role in determining ER morphology.

Keywords: endoplasmic reticulum/FFAT motif/ORP proteins/VAP-33 proteins

Introduction

The endoplasmic reticulum (ER) is a multi-functional organelle. After translocation across the ER membrane, secreted proteins fold, undergo post-translational modification and assemble into multi-protein complexes in the ER lumen (Baumann and Walz, 2001). Additionally, the cytosolic surface of the ER membrane is a major site for lipid biosynthesis, and many peripheral membrane proteins are localized to the cytosolic surface of the ER membrane (Baumann and Walz, 2001). While the mechanism by which proteins are targeted for translocation into the ER lumen is well characterized, it is not well understood how proteins are targeted to the cytosolic surface of the ER. Recent work has identified a targeting signal (the FFAT motif) responsible for targeting cytosolic proteins to the surface of the ER (Loewen et al., 2003) and to the nuclear membrane (Brickner and Walter, 2004). The FFAT motif has the consensus amino acid sequence EFFDAxE (Loewen et al., 2003). This motif was identified because it is conserved in a large family of Oxysterol Binding Protein Related Proteins (ORPs) (Figure 1A and Supplemental Figure 1A) (Loewen et al., 2003). ORPs are regulators of lipid metabolism that are targeted by their FFAT motifs to the cytosolic surface of the ER (Loewen et al., 2003). In both yeast and mammals, proteins containing exposed FFAT motifs are targeted to ER membranes by interactions with VAP proteins (Loewen et al., 2003; Wyles et al., 2002).

VAP proteins are type-IV transmembrane proteins composed of 3 conserved domains. These include an N-terminal immunoglobulin-like beta sheet, a central coiled-coil domain, and a C-terminal transmembrane domain (Figure 1A). The N-terminal domain shares 22% sequence identity with the well characterized Major Sperm Protein (MSP) (Figure 1A and Supplemental Figure 1B) (Roberts and Stewart, 2000). However, it is unclear whether VAP proteins share a common function. In metazoans, in addition to its role in recruiting FFAT motif-targeted

proteins to ER membranes (Brickner and Walter, 2004; Kagiwada et al., 1998; Loewen and Levine, 2005; Loewen et al., 2003; Skehel et al., 2000; Soussan et al., 1999; Wyles et al., 2002; Wyles and Ridgway, 2004), VAP has been proposed to function in vesicle trafficking (Amarilio et al., 2005; Foster et al., 2000; Skehel et al., 1995), and in the organization of microtubule networks (Amarilio et al., 2005; Pennetta et al., 2002). Scs2p, the yeast homologue of VAP, binds FFAT motifs, and yeast lacking Scs2p mislocalize FFAT-targeted proteins to the cytoplasm (Loewen et al., 2003). In addition to its role in recruiting ORPs to the ER, Scs2p has also been implicated in transcriptional regulation of the INO1 gene that encodes an important phospholipid biosynthetic protein (Brickner and Walter, 2004; Kagiwada et al., 1998). Strains lacking *SCS2* are unable to activate the *INO1* gene and cannot grow in the absence of inositol. Opi1p, a transcriptional repressor of *INO1* that possesses an FFAT motif (Figure 1A), is regulated by Scs2p on the nuclear membrane (Brickner and Walter, 2004; Loewen et al., 2003).

Here we present the crystal structure for a VAP-FFAT motif interaction. We find that the specific molecular interactions between FFAT and VAP are highly conserved from yeast to mammals. Based on our structure of the VAP-FFAT complex we designed mutants of the yeast VAP homologue Scs2p that are defective for FFAT motif binding. These mutants were defective for activation of *INO1*, indicating that FFAT-mediated binding of Scs2p to Opi1p is essential for this activation event. Finally, overexpression of wild-type VAP or of VAP defective for FFAT binding alters ER morphology in distinct patterns, suggesting that VAP and FFAT-proteins play an important role in maintaining ER morphology.

Results and Discussion

VAP Interacts With Proteins Containing FFAT Motifs

To investigate VAP function, we analyzed the ability of VAP proteins to interact with putative binding partners that were suggested in previous reports (Pennetta et al., 2002; Skehel et al., 2000; Weir et al., 2001; Wyles et al., 2002). We were able to reproduce the reported interaction between VAP homologues and proteins containing FFAT motifs (Loewen and Levine, 2005; Loewen et al., 2003) with purified proteins *in vitro*. However, we found no evidence for direct interactions of cytosolic portions of VAP with cytosolic portions of SNARE proteins or with tubulin or microtubules (data not shown). The stoichiometry of VAP-FFAT interaction was determined by size exclusion chromatography coupled to in-line multi-angle laser light scattering (SEC-MALLS); recombinant rat ORP1 (454-546) (which contains the ORP1 FFAT motif) interacts with rat VAP (1-125) in a 1:1 complex (Supplemental Figure 2). The interaction between VAP proteins and FFAT motifs was also confirmed by a native gelshift assay (Figure 1B). VAP (1-125) alone (lane 1) migrates at a different rate from VAP (1-125) plus equimolar amounts of the ORP1 FFAT peptide SEDEFYDALS (lane 2). We obtained similar results for the yeast Scs2p:Opi1p interaction (Figure 1B).

Crystal Structure of the rat VAP-A MSP homology domain

To find a stable fragment of VAP-A that would be suitable for crystallography, we performed limited trypsin digestion of the cytosolic portion of rat VAP-A (residues 1-219). We obtained a stable fragment consisting of VAP-A residues 1-123 as measured by MALDI mass spectrometry (data not shown). Secondary structure predictions (Rost and Liu, 2003) suggest that VAP-A residue 125 is the end of the beta strand that contains residue 123. We thus expressed, purified and crystallized VAP (1-125).

The crystal structure of selenomethionine-substituted rat VAP-A (1-125) was solved to 1.7 Å resolution using data from a multiwavelength anomalous dispersion (MAD) experiment

(Table 1) (Hendrickson, 1991). As expected from sequence homology, the fold of VAP-A (1-125) is the same as that of MSP. Both are seven-stranded immunoglobulin-like β-sandwiches with s-type topology and their C_α backbones align with an r.m.s.d. of 2.0 Å over 109 residues (Bullock et al., 1996). Although they share the same fold and 22% sequence identity, VAP (1-125) and MSP have distinct surface electrostatic properties (Figure 2) and behave differently in solution. While MSP forms a symmetric dimer (Figures 2C and 2D) with a K_d of less than 50 nM (Haaf et al., 1996), VAP (1-125) is monomeric in solution as measured by SEC-MALLS (Supplemental Figure 2). VAP (1-125) crystallizes with one molecule in the asymetric unit, but forms a symmetric crystal contact across a crystallographic two-fold interface with a buried surface area of 440 $Å^2$. This interface is centered on a highly conserved sequence that contains Cys53. In approximately 50% of the crystal, Cys53 residues are disulfide bonded across this crystallographic interface, likely representing an artifact of crystallization. It is therefore noteworthy that VAP (1-125) is monomeric in solution and that at the high protein concentration required for crystallization, none of the crystal contacts correspond to the MSP dimer interface. Indeed, critical residues in the MSP dimerization interface, such as Val18 and Tyr29, are not conserved in VAP (1-125) (Bullock et al., 1996). These residues are instead replaced in VAP-A by polar residues Lys17 and Thr28 (Bullock et al., 1996). We conclude that VAP (1-125) does not dimerize in the same way as MSP.

Crystal Structure of a VAP-FFAT complex

We next sought to determine the structural basis for the interaction between VAP proteins and FFAT motifs. We solved the structure of rat VAP-A (1-125) in complex with the rat ORP1 FFAT motif (residues 472-SEDEFYDALS-481) using diffraction data from a single wavelength anomalous dispersion (SAD) experiment and a 1.9 Å native data set (Table 2)

(Hendrickson, 1991). The structure of VAP (1-125) is subtly changed by FFAT binding. VAP C_α backbones from our structures align with an r.m.s.d. of 1.3 Å over 113 residues. The FFAT motif binds across VAP beta strands F, E, C, and D1 (Figure 3A). FFAT binding causes small (0.1-0.5 Å) changes in the position of backbone atoms within these strands and substantial changes (2-4 Å) in the position of several side-chain atoms that accommodate FFAT binding. We observe clear electron density for main and side chain atoms of ORP1 FFAT residues 476-481 and main chain atoms of residues 473-475 (Figure 3B). The FFAT residue Phe476 binds VAP in a hydrophobic pocket created by the aliphatic amino acid side chains of several residues (Figure 3B). It has extensive hydrophobic Van der Waals contacts with VAP-A residue Met89 and with aliphatic portions of side chains from VAP-A residues Lys45, Thr47, Lys87 and Lys118 (Figure 3B).

The FFAT motif binds VAP on a positive patch that is in a highly conserved region on the VAP protein surface (Figures 3C and 3D). Part of the FFAT binding site on the yeast VAP homologue Scs2p was recently identified by a mutagenic screen (Loewen and Levine, 2005). This screen identified residues equivalent to VAP-A Lys45, Thr47, Lys87 and Lys118 as essential for VAP-FFAT interactions. Our structure reveals that rather than interacting with negative side chains in FFAT motifs, aliphatic portions of these side chains form part of the hydrophobic pocket where FFAT residue Phe476 binds. Additionally, our structure shows the full complement of VAP-FFAT interactions. FFAT residues 477 and 479-481 are bound to VAP by a network of backbone – backbone hydrogen bonds. Although the FFAT consensus sequence is EFFDAxE, the rat ORP1 FFAT sequence has the sequence 472-SEDEFYDALS-481. In our structure, FFAT residue Tyr479 is ordered but lacks substantial interactions with VAP. It is restrained by weak Van der Waals interactions with several residues and its gamma hydroxyl

group lacks a hydrogen bonding partner. This lack of strong interactions explains the observed variation between Phe or Tyr in the FFAT proteins identified to date and suggests that FFAT sequences with other residues at this position may be able to bind VAP. The side chain of Ala479 binds VAP in a small hydrophobic pocket created by aliphatic portions of side chains from residues Val44, Thr46, and Val54.

Although VAP (1-125) interacts with an FFAT motif as a 1:1 complex as determined by SEC-MALLS (Supplemental Figure 2), VAP-FFAT crystals are composed of two VAP MSP domains with two FFAT motifs bound between them (Figures 4A and 4B). As measured by SEC-MALLS, the VAP coiled-coil domain causes dimerization of VAP (1-219) (data not shown). The transmembrane domain, which contains the dimerization motif GxxxG (Russ and Engelman, 2000), is also likely to drive VAP dimerization. Thus, the observed crystal packing may mimic the high local VAP (1-125) concentration that would result from coiled-coil and transmembrane domain induced VAP dimerization. Several additional observations corroborate this hypothesis. The VAP-VAP, VAP-FFAT, and FFAT-FFAT interactions within the 2:2 complex bury 1700 $Å^2$ of surface area and may explain the conservation of residues in FFAT motifs that are not explained by the 1:1 VAP-FFAT complex alone (Figure 4). In particular, of the residues in the EFFDAxE FFAT consensus sequence, the Asp following the single ring aromatic residues in FFAT motifs (Asp478 in ORP1) is strictly conserved among FFAT proteins identified to date (Supplemental Figure 1A). Asp478 forms symmetric hydrogen bonds between the two FFAT motifs within a 2:2 complex (Figure 4C). These symmetric hydrogen bonds may explain the high conservation of Asp478 in FFAT motifs (Supplemental Figure 1A). As described above, the side-chain of FFAT residue Tyr477 is only weakly restrained by the VAP surface to which it is primarily bound. This residue is further restrained by hydrophobic Van der

Waals contact with an aliphatic portion of the Asp478 side chain from the second FFAT motif within a 2:2 complex. Another argument for the relevance of the 2:2 complex is that it could form in the context of full-length VAP and full-length ORP1. The C-termini of the two VAP (1-125) domains project from the same face of a 2:2 complex (Figure 4A). The termini of the bound ORP1 peptide are oriented in a way that is consistent with VAP on membranes binding an FFAT motif of a large cytosolic protein (Figure 4A and 4B). Thus, the 2:2 complex could form between full-length VAP and FFAT proteins with both VAP coiled-coil domains dimerized and both VAP molecules tethered to the same membrane by their C-terminal transmembrane domains (Figure 4A).

FFAT binding is a conserved VAP function

The FFAT motif binding site is highly conserved among VAP protein family members but is not conserved in the structurally similar MSP-1 (Figure 3D). This observation prompted us to assess whether the yeast VAP homologue Scs2p interacts with FFAT motifs using the same molecular mechanism as rat VAP-A and to assess the functional significance of FFAT interactions for Scs2p function. We used the structure of the VAP-FFAT complex to construct point mutations on the surface of rat VAP-A that we predicted would specifically prevent FFAT binding. We chose to mutate two residues on the VAP surface that interact with FFAT residue Phe476 (Figure 3B) to acidic residues by making the double point mutation K87D/M89D. As expected, in a native gel, the band corresponding to VAP (1-125) K87D/M89D double mutant does not shift upon addition of the FFAT peptide (compare Figure 1B lanes 3 and 4). Wild-type and mutant VAP (1-125) are both folded as measured by circular dichroism and are both monodisperse and monomeric in solution as measured by SEC-MALLS (data not shown).

Mutating the homologous residues (K84D/L86D) in the yeast VAP homologue, Scs2p,

disrupted Scs2p interactions with the FFAT motif of the yeast protein Opi1p *in vitro* (Figure 1B). The gel shift experiments confirm that Scs2p residues K84 and L86 are equivalent to rat VAP-A residues K87 and M89 and that both proteins probably bind to FFAT motifs by the same mechanism. We next tested if the K84D/L86D mutant of Scs2p was functional in yeast. Strains lacking *SCS2* are unable to activate *INO1* and cannot grow in the absence of inositol. Expression of wildtype Scs2p in an *scs2*Δ mutant strain allowed activation of *INO1* and growth on medium lacking inositol. In contrast, Scs2p K84D/L86D failed to complement this growth phenotype (Figure 5A). Western blot analysis of total protein from yeast strains expressing wildtype or mutant Scs2p confirmed that the K84D/L86D mutant was expressed and stable in yeast (Figure 5B). Thus, the essential function of Scs2p in activating *INO1* requires its evolutionarily conserved FFAT binding activity.

Overexpression of VAP or an FFAT binding mutant causes altered ER morphology

Several recent reports suggest that VAP-FFAT interactions may regulate ER morphology (Amarilio et al., 2005; Wyles et al., 2002; Wyles and Ridgway, 2004). VAP (1-242) overexpressed in COS7 cells as a C-terminal GFP fusion protein is localized to perinuclear and ER membranes and overlays with staining of the ER marker calreticulin (Figure 6A) but not with microtubules (Figure 6B). VAP-GFP overexpression resulted in the range of ER phenotypes illustrated in Figures 6A-6E. Overexpression of the VAP (1-242) K87D/M89D mutant, which disrupts FFAT binding, resulted in a range of ER phenotypes ranging from those seen with overexpression of wild-type VAP to, in approximately 1-10% of transfected cells, a pattern of regularly-spaced patches of increased fluorescence as shown in Figures 6G and 6H. These patches are continuous with normal-appearing reticulated ER and colocalize with ER markers. This regular pattern of dense patches was never observed with overexpression of wild-type VAP.

Since the K87D/M89D double point mutation does not affect VAP folding and structure it is likely that the observed pattern of dense patches results from the disruption of VAP-FFAT interactions.

Implications of the VAP-FFAT interaction

The VAP-FFAT co-crystal structure reveals the structural basis for VAP binding of FFAT motif containing proteins. We used the VAP-FFAT structure to design a stable VAP double point mutant that, although properly folded, is unable to bind FFAT motifs. We used this mutant to functionally characterize VAP-FFAT interactions and their conservation. We also characterized the effects of VAP protein overexpression on ER morphology in COS7 cells.

The VAP-FFAT structure should facilitate analysis of future questions concerning VAP interactions with FFAT motifs or with other proteins. For instance, we predict that a human isoform of VAP, VAP-C, is unable to bind FFAT motifs. Among other changes, VAP-C replaces Lys87 with His and Met89 with Ser. These changes are strikingly similar to the K87D/M89D mutant that we have shown does not bind FFAT motifs.

It is conceivable that FFAT proteins compete for VAP interactions. Thus, the primary sequence variability and the relative affinities of various FFAT motifs (Supplemental Figure 1A) that bind VAP proteins need to be analyzed. Our VAP-FFAT structure explains much of the primary sequence conservation observed in FFAT motifs. The primary VAP-FFAT interaction includes the first single ring aromatic residue in the EFFDAxE FFAT consensus sequence that binds in a hydrophobic cavity on VAP. The orientation of Phe476 in our structure suggests the possibility that FFAT motifs with Tyr at this position may still bind in a similar fashion. The secondary interactions in the 2:2 complex observed in VAP-FFAT crystals explain the high conservation of the Asp residue in the EFFDAxE FFAT consensus sequence. It is also

noteworthy that the sidechain for the first Glu in the EFFDAxE FFAT consensus sequence is not ordered in our structure. This may suggest that this residue is not absolutely conserved in FFAT motifs. Similarly, there are a variety of potential hydrogen bonding partners for the final Glu in the EFFDAxE FFAT consensus sequence. This coincides with the observed sequence heterogeneity within previously identified FFAT motifs. We propose that a less stringent definition of this motif sequence is required and that a wider variety of cytosolic proteins may be targeted to VAP on ER membranes than has been anticipated.

Experimental Procedures

Expression and Purification: DNAs encoding Rattus norvegicus VAP-A and OSBP-L1a Δ41-130 were cloned using standard methodology from a brain cDNA library (Clonetech) and inserted into the pCR-Blunt II – TOPO vector (Invitrogen). Fragments corresponding to VAP amino acid residues 1-125 and 1-219 and OSBP-L1a residues 454-546 were subcloned into the pGEX-4T expression vector (Pharmacia) and sequenced. Residues 1-125 or 1-219 of rat VAP or residues 454-546 of OSBP-L1a were expressed as N-terminal glutathione-S-transferase (GST) fusion proteins in *E. coli*. BL21 (Novagen) cells were transformed with expression vector and grown in a BIOFLO3000 fermenter (New Brunswick) to OD_{600} 30 in ECPYM1 media (Bernard and Payton, 1995) with 0.1 mg/mL ampicllin at 37 ^{o}C. The temperature was shifted to 30 ^{o}C and heterologous protein expression was then initiated with 1 mM IPTG for 4 hours. Cells were harvested, flash frozen in liquid nitrogen, and stored at –80 ^{o}C for later use. Selenomethionine substituted protein was prepared by growing BL21 cells in M9 minimal media and inhibiting methionine biosynthesis in the presence of selenomethionine as described (Van Duyne et al., 1993). Expression was induced from the pGEX-4T vector by addition of 1 mM IPTG after the

temperature was shifted from 37 ^{o}C to 30 ^{o}C at OD_{600} 1.5. After 4 hours of induction cells were harvested, flash frozen and stored for later use. For protein purification, 30 grams of frozen bacterial cells were resuspended in 200 mL of lysis buffer consisting of 50 mM Tris (pH 8.0), 250 mM NaCl, 5 mM EDTA and 10 mM DTT and lysed using a pneumatic cell cracker at 16,000 PSI (Microfluidics). The lysate was then centrifuged in a JA-14 rotor (Beckman) at RCF (avg) 18,879 for 60 minutes and the supernatant was incubated in batch with glutathione-sepharose resin (Pharmacia) at 4 ^{o}C for 1 hour with gentle stirring. Fusion proteins were retained on the beads and were washed 3 times with 4 bed volumes of lysis buffer then 3 times with 4 bed volumes of thrombin buffer (50 mM Tris pH 8.0, 250 mM NaCl, 13 mM 2-mercaptoethanol, 5 mM $CaCl_2$). The beads were then resuspended with thrombin buffer and incubated with ~50 μg of bovine α-thrombin (Haematologic Technologies) at 4 ^{o}C for 6 hours with slow mixing by rotation. After thrombin cleavage the VAP or ORP1 protein containing supernatants were dialyzed into 20 mM MES buffer pH 6, 50 mM NaCl, 13 mM BME and were loaded onto a 10/10 mono-S (Pharmacia) column and eluted with a linear gradient of sodium chloride from 50 mM to 500 mM. VAP or ORP1 proteins were further purified by gel filtration chromatography on a pharmacia Superdex 75 16/60 column then dialyzed into milli-Q water with 10 mM DTT and concentrated to 25 mg/mL before flash freezing 50 uL aliquots in liquid nitrogen for storage at –80 ^{o}C. Protein concentrations were calculated from absorbance measurements under denaturing conditions using theoretical molar extinction coefficients.

Peptides corresponding to rat OSBP-L1a residues 472-481 (SEDEFYDALS) and yeast Opi1p residues 197-206 (DDEEFFDASE) were synthesized by Biopeptide LLC. Peptides were resuspended in water before flash freezing small aliquots for later use.

Yeast Scs2p genomic DNA was amplified from genomic DNA and inserted into the pCR-Blunt II – TOPO vector (Invitrogen). A fragment corresponding to Scs2p amino acid residues 1-224 was subcloned into the pet28c expression vector (Pharmacia) and sequenced. Scs2p (1-224) was expressed as an N-terminal 6xHis fusion protein in *E. coli*. BL21 (DE3) cells were transformed with expression vector and grown to OD_{600} 1.5 in LB medium with 0.1 mg/mL kanamycin at 37 ^{o}C. The temperature was shifted to 30 ^{o}C and heterologous protein expression was then initiated with 1 mM IPTG for 5 hours. Cells were harvested, flash frozen in liquid nitrogen, and stored at –80 ^{o}C for later use. For protein purification, cells were resuspended in lysis buffer consisting of 50 mM HEPES (pH 7.5), 150 mM NaCl, and 10 mM 2-mercaptoethanol and lysed using a pneumatic cell cracker at 16,000 PSI (Microfluidics). The lysate was then centrifuged in a JA-14 rotor (Beckman) at RCF (avg) 18,879 for 60 minutes and the supernatant was incubated in batch with Ni-NTA resin (Qiagen) at 4 ^{o}C for 2 hours with gentle mixing. Fusion proteins were retained on the beads and were washed 3 times with 4 bed volumes of lysis buffer plus 20 mM imidazole then 3 times with 4 bed volumes of elution buffer (50 mM HEPES pH 7.5, 150 mM NaCl, 10 mM 2-mercaptoethanol, 200 mM imidazole). Fractions containing fusion protein were then pooled and dialyzed into 50 mM HEPES pH 7.5, 10 mM 2-mercaptoethanol overnight in the presence of ~50 μg of bovine α-thrombin (Amersham Bioechnologies). Cleaved Scs2p protein was loaded onto a fast flow Hi-Trap Q (Pharmacia) column and eluted with a linear gradient of sodium chloride from 100 mM to 200 mM. Scs2p protein containing fractions were pooled before flash freezing 25 uL aliquots in liquid nitrogen for storage at –80 ^{o}C.

Protein Crystallization: Selenomethionine substituted VAP (1-125) was thawed and crystals were grown by vapor diffusion using sitting drops formed by mixing a 1:1 volume ratio of

25mg/mL VAP with an equilibration buffer consisting of 30% polyethylene glycol monomethetheyl ether molecular weight 2000, 200 mM NaCl, 25 mM Tris buffer pH 7.5. Crystals formed over 1-3 weeks at 10 ^{o}C in the space group $P4_22_12$ with unit cell dimensions a=b=45 Å, c=112 Å and contained one molecule per asymmetric unit with 45% solvent. For crystallization of the VAP-FFAT motif complex, a 2:1 molar ratio of peptide to VAP (1-125) was mixed to produce a protein solution with 2.5 mM peptide, 1.25 mM VAP, 6.8 mM DTT, 6.4 mM PIPES pH 7.4. A small initial crystal grew in Hampton Research screen IndexHT condition H11 and subsequent crystals were grown by vapor diffusion using macroseeded sitting drops formed by mixing a 1:1 volume ratio of protein solution with an equilibration buffer consisting of 27% polyethylene glycol monomethetheyl ether molecular weight 2000, 100 mM sodium thiocyanate, 100 mM Tris buffer pH 7.4. Crystals formed in space group P1 with unit cell dimensions a=50.1 Å, b=50.0 Å, c=90.3 Å, α=90.0^{o}, β=90.0^{o}, γ=60.0^{o} and contained 6 molecules per asymmetric unit with 45% solvent.

Crystallographic Data Collection: Crystals were removed from sitting drops with a nylon loop and transferred to a cryoprotectant solution composed of equilibration buffer supplemented with 15% ethylene glycol. Crystals were then cryocooled directly in a 100 K cryostream and diffraction data were collected at beamline 8.2.1 of the Advanced Light Source using an ADSC Quantum-210 CCD detector. For the VAP (1-125) MAD experiment oscillation data were collected using inverse beam geometry in 15^{o} wedges with all three wavelengths collected for each wedge simultaneously. For the VAP-FFAT complex moderate resolution SAD oscillation data were collected at the Selenium peak wavelength using inverse beam geometry in 5^{o} wedges and a 1.9 Å resolution native data set was also collected. Diffraction data were processed using

Mosflm/Scala (Collaborative.Computational.Project.Number.Four, 1994). Data statistics are summarized in Tables 1 and 2.

Structure Determination and Refinement: For VAP (1-125) the six expected selenium sites were found in anomalous difference Patterson maps calculated using the peak wavelength with an automated Patterson heavy atom search method (Grosse-Kunstleve and Brunger, 1999). MAD phasing and density modification were carried out in CNS (Brunger et al., 1998) and resulted in a readily interpretable experimental electron density map. A partial model was built automatically with wARP (Perrakis et al., 1999), and the remainder of the model was built using the program O (Jones et al., 1991). Model refinement was monitored using the free R value (Brunger, 1992) computed from a randomly omitted 10% of the observed diffraction data. Refinement was carried out in CNS using alternating rounds of simulated annealing, torsion angle molecular dynamics (Rice and Brunger, 1994), restrained B factor refinement (Hendrickson, 1985), and model rebuilding. The final model contains one N-terminal vector derived residue followed by residues 1-125 of VAP. The final model has excellent stereochemistry (no residues in the disallowed region of the Ramachandran plot), and R/R_{free} values of 22.1% and 24.2%, respectively.

The VAP-FFAT complex crystallized in space group P1. Although data could be processed in space group P3(2)21, a 1 Å translation along Z for molecules obeying the symmetry operators [x-y, -y, -z+1/3], [-x, -x+y, -z-1/3], or [y, x, -z] caused refinement to converge poorly. Electron density for the bound FFAT peptide was clear and refinement proceeded normally in space group P1. The 36 selenium sites from the 6 VAP molecules in the P1 cell were found by molecular replacement using the VAP (1-125) model in CNS. SAD phasing and density modification were carried out in CNS using a molecular envelope generated with the VAP (1-

125) coordinates using MAMA (Kleywegt and Jones, 1999). Density modified SAD phases were of reasonable quality. Native data extended to 1.9 Å and after minor rebuilding of the VAP (1-125) model and addition of residues from the FFAT peptide, refinement was carried out in CNS with SAD experimental phases as outlined above. The bulk anisotropic B factor was somewhat high and addition of individual restrained B factors showed no improvement over group restrained B-factor refinement. Translation, libration, and screw-rotation (TLS) refinement (Winn et al., 2001) in REFMAC with 6 TLS groups, each consisting of a VAP (1-125) domain with bound peptide, improved both R_{free} and R values by 3-4%. Tight NCS restraints were used for all atoms throughout refinement. The final model contains VAP residues 4-125 and OSBP-L1a residues 473-481. Two residues had uninterpretable electron density. VAP residues 98-99 have their occupancies set to zero and ORP1 residues 473-475 were modeled as alanines. The final model has no residues in the disallowed region of the Ramachandran plot and R/R_{free} values of 23% and 26%, respectively. Molecular graphics were generated with Pymol (DeLano, 2002).

Gel Shift Assay: Native gel electrophoresis was carried out using 8–25% native Phast (Pharmacia) gels with native buffer strips (0.88 M L-alanine, 0.25 M Tris, pH 8.8, and 1 mM EDTA). Samples were mixed and incubated for at least 30 minutes in 50 mM Hepes, pH 7.5, 150 mM NaCl, 5 mM DTT before loading the gel.

Yeast Growth Assay: SCS2 was amplified from genomic DNA with upstream primer GTCAGAGCACTGAACGAGG and downstream primer CGCCTACTACACTAGGGAAACC. The PCR product contained the SCS2 cDNA sequence (CDS), plus 506 bp upstream and 287 bp downstream of the SCS2 gene. The PCR product was first inserted into the pCR-Blunt II – TOPO vector (Invitrogen) and then subcloned as an EcoRI fragment into pRS313 (Sikorski and

Hieter, 1989) and sequenced. Yeast growth assays were performed by making a suspension of ~2 x 10^7 cells per mL and a series of 10-fold dilutions were spotted onto SDC –inositol - histidine medium and incubated at 37 ^{o}C for two days.

Fluorescence microscopy and image processing: For experiments in COS7 cells, full-length rat VAP-A (residues 1-242) was subcloned as an XhoI – HindIII fragment in pEGFP-N1 (CLONTECH) and confirmed by sequencing. COS7 cells were grown in DMEM with 10% serum. Cells were transfected with Lipofectamine 2000 and plated on collagen-coated glass coverslips. Cells were fixed 48 hours after transfection in 4% paraformaldehyde or 0.3% glutaraldehyde for costaining of microtubules. For tubulin staining, DM1α (Sigma) was used at 1/500. Polyclonal antibodies to calnexin and calrecticulin were diluted 1/1000 (Stressgen). Cells were mounted in Vectashield mounting medium or Vectashild with DAPI (Vector Laboratories, Inc. Burlingame, CA). Image z-stacks were collected in 0.20 µm steps on an Olympus IX-70 inverted microscope with a 60x 1.4 N.A. oil-immersion objective (Olympus Corp.), and captured by a cooled CCD camera (Photometrics Ltd.). Images were collected and processed using Delta Vision deconvolution software (Applied Precision, Inc., Seattle, WA) on a Silicon Graphics workstation (Silicon Graphics Corp).

Acknowledgements

We thank L. Rice for advice on SAD data collection, R. Grosse-Kunstleve, N. Sauter and P. Adams for advice while solving the structures, and D. Starcevic, M. Bowen, M. Breidenbach, J. Hyman, S. Fukai, R. Reimer, D. Hattendorf, K. Slep, S. Jaswal, J. Kohler, J. Christianson, R. Kopito, and J. Nelson for discussions and critical reading of the manuscript.

The diffraction data used in this paper were collected at the Lawrence Berkeley National Laboratory Advanced Light Source beamline 8.2.1. We thank Corie Ralston for generous assistance with data collection. Portions of this research were carried out at the Stanford Synchrotron Radiation Laboratory, a national user facility operated by Stanford University on behalf of the US Department of Energy (Office of Basic Energy Sciences). The SSRL Structural Molecular Biology Program is supported by the Department of Energy (Office of Biological and Environmental Research) and by the National Institutes of Health (National Center for Research Resources, Biomedical Technology Program).

References

Amarilio, R., Ramachandran, S., Sabanay, H. and Lev, S. (2005) Differential regulation of ER structure through VAP-Nir protein interaction. *J Biol Chem*, **280**, 5934-5944.

Baumann, O. and Walz, B. (2001) Endoplasmic reticulum of animal cells and its organization into structural and functional domains. *Int Rev Cytol*, **205**, 149-214.

Bernard, A. and Payton, M. (1995) Fermentation and growth of *Escherichia coli* for optimal protein production. *Current Protocols in Protein Science*, **5**, 1-18.

Brickner, J.H. and Walter, P. (2004) Gene Recruitment of the Activated *INO1* Locus to the Nuclear Membrane. *PLoS Biol*, **2**, E342.

Brunger, A. (1992) The free R value: a novel statistical quantity for assessing the accuracy of crystal structures. *Nature*, **355**, 472-474.

Brunger, A.T., Adams, P.D., Clore, G.M., DeLano, W.L., Gros, P., Grosse-Kunstleve, R.W., Jiang, J.S., Kuszewski, J., Nilges, M., Pannu, N.S., Read, R.J., Rice, L.M., Simonson, T. and Warren, G.L. (1998) Crystallography & NMR system: A new software suite for macromolecular structure determination. *Acta Crystallogr D Biol Crystallogr*, **54**, 905-921.

Bullock, T.L., Roberts, T.M. and Stewart, M. (1996) 2.5 A resolution crystal structure of the motile major sperm protein (MSP) of Ascaris suum. *J Mol Biol*, **263**, 284-296.

Collaborative.Computational.Project.Number.Four. (1994) The CCP4 suite: programs for protein crystallography. *Acta Crystallogr. D Biol. Crystallogr.*, **50**, 760-763.

DeLano, W.L. (2002) The PyMOL Molecular Graphics System. *on World Wide Web* *http://www.pymol.org*.

Foster, L.J., Weir, M.L., Lim, D.Y., Liu, Z., Trimble, W.S. and Klip, A. (2000) A functional role for VAP-33 in insulin-stimulated GLUT4 traffic. *Traffic*, **1**, 512-521.

Grosse-Kunstleve, R.W. and Brunger, A.T. (1999) A highly automated heavy-atom search procedure for macromolecular structures. *Acta Crystallogr D Biol Crystallogr*, **55 (Pt 9)**, 1568-1577.

Haaf, A., Butler, P.J., Kent, H.M., Fearnley, I.M., Roberts, T.M., Neuhaus, D. and Stewart, M. (1996) The motile major sperm protein (MSP) from Ascaris suum is a symmetric dimer in solution. *J Mol Biol*, **260**, 251-260.

Hendrickson, W.A. (1985) Stereochemically restrained refinement of macromolecular structures. *Methods Enzymol*, **115**, 252-270.

Hendrickson, W.A. (1991) Determination of macromolecular structures from anomalous diffraction of synchrotron radiation. *Science*, **254**, 51-58.

Jones, T.A., Zou, J.Y., Cowan, S.W. and Kjeldgaard. (1991) Improved methods for building protein models in electron density maps and the location of errors in these models. *Acta Crystallogr A*, **47 (Pt 2)**, 110-119.

Kagiwada, S., Hosaka, K., Murata, M., Nikawa, J. and Takatsuki, A. (1998) The Saccharomyces cerevisiae SCS2 gene product, a homolog of a synaptobrevin-associated protein, is an integral membrane protein of the endoplasmic reticulum and is required for inositol metabolism. *J Bacteriol*, **180**, 1700-1708.

Kleywegt, G.J. and Jones, T.A. (1999) Software for handling macromolecular envelopes. *Acta Crystallogr D Biol Crystallogr*, **55 (Pt 4)**, 941-944.

Loewen, C.J. and Levine, T.P. (2005) A highly conserved binding site in VAP for the FFAT motif of lipid binding proteins. *J Biol Chem*.

Loewen, C.J., Roy, A. and Levine, T.P. (2003) A conserved ER targeting motif in three families of lipid binding proteins and in Opi1p binds VAP. *Embo J*, **22**, 2025-2035.

Pennetta, G., Hiesinger, P., Fabian-Fine, R., Meinertzhagen, I. and Bellen, H. (2002) Drosophila VAP-33A directs bouton formation at neuromuscular junctions in a dosage-dependent manner. *Neuron*, **35**, 291-306.

Perrakis, A., Morris, R. and Lamzin, V.S. (1999) Automated protein model building combined with iterative structure refinement. *Nat Struct Biol*, **6**, 458-463.

Rice, L.M. and Brunger, A.T. (1994) Torsion angle dynamics: reduced variable conformational sampling enhances crystallographic structure refinement. *Proteins*, **19**, 277-290.

Roberts, T.M. and Stewart, M. (2000) Acting like actin. The dynamics of the nematode major sperm protein (msp) cytoskeleton indicate a push-pull mechanism for amoeboid cell motility. *J Cell Biol*, **149**, 7-12.

Rost, B. and Liu, J. (2003) The PredictProtein server. *Nucleic Acids Res*, **31**, 3300-3304.

Russ, W.P. and Engelman, D.M. (2000) The GxxxG motif: a framework for transmembrane helix-helix association. *J Mol Biol*, **296**, 911-919.

Sikorski, R.S. and Hieter, P. (1989) A system of shuttle vectors and yeast host strains designed for efficient manipulation of DNA in Saccharomyces cerevisiae. *Genetics*, **122**, 19-27.

Skehel, P.A., Fabian-Fine, R. and Kandel, E.R. (2000) Mouse VAP33 is associated with the endoplasmic reticulum and microtubules. *Proc Natl Acad Sci U S A*, **97**, 1101-1106.

Skehel, P.A., Martin, K.C., Kandel, E.R. and Bartsch, D. (1995) A VAMP-binding protein from Aplysia required for neurotransmitter release. *Science*, **269**, 1580-1583.

Soussan, L., Burakov, D., Daniels, M.P., Toister-Achituv, M., Porat, A., Yarden, Y. and Elazar, Z. (1999) ERG30, a VAP-33-related protein, functions in protein transport mediated by COPI vesicles. *J Cell Biol*, **146**, 301-311.

Van Duyne, G.D., Standaert, R.F., Karplus, P.A., Schreiber, S.L. and Clardy, J. (1993) Atomic structures of the human immunophilin FKBP-12 complexes with FK506 and rapamycin. *J Mol Biol*, **229**, 105-124.

Weir, M.L., Xie, H., Klip, A. and Trimble, W.S. (2001) VAP-A binds promiscuously to both v- and tSNAREs. *Biochem Biophys Res Commun*, **286**, 616-621.

Winn, M.D., Isupov, M.N. and Murshudov, G.N. (2001) Use of TLS parameters to model anisotropic displacements in macromolecular refinement. *Acta Crystallogr D Biol Crystallogr*, **57**, 122-133.

Wyles, J.P., McMaster, C.R. and Ridgway, N.D. (2002) Vesicle-associated membrane protein-associated protein-A (VAP-A) interacts with the oxysterol-binding protein to modify export from the endoplasmic reticulum. *J Biol Chem*, **277**, 29908-29918.

Wyles, J.P. and Ridgway, N.D. (2004) VAMP-associated protein-A regulates partitioning of oxysterol-binding protein-related protein-9 between the endoplasmic reticulum and Golgi apparatus. *Exp Cell Res*, **297**, 533-547.

Figure Legends

Figure 1. Domain diagrams and sequence alignments for proteins studied in this paper.

(A) Domain organization diagrams of VAP, ORP1 and Opi1p. Domain abbreviations are: Major Sperm Protein Homology Domain, MSP; coiled-coil domain, CC; transmembrane domain, T; ankyrin repeats, ANK; Plekstrin homology domain, PH; FFAT motif with sequence related to EFFDAxE (Loewen et al., 2003), F; OSBP related protein lipid binding domain, ORP; Sin3p binding domain, S; basic leucine zipper, Z.

(B) Native gelshift assay. VAP (1-125) alone (lane 1) migrates at a different rate from VAP (1-125) plus equimolar amounts of the ORP1 FFAT peptide SEDEFYDALS (lane 2) demonstrating that VAP (1-125) binds FFAT motifs directly. VAP (1-125) K87D/M89D migrates faster than VAP (1-125) (lanes 1 and 3). The mobility of VAP(1-125) K87D/M89D is not affected by added FFAT motif (lanes 3 and 4) suggesting that VAP K87D/M89D does not bind FFAT motifs. Yeast Scs2p binds to the FFAT motif peptide from yeast Opi1p (lanes 5 and 6). The yeast Opi1p peptide DDEEFFDASE caused a mobility shift of Scs2p (1-224) (lanes 5 and 6). The mobility of Scs2p (1-224) K84D/L86D is not affected by added peptide (lanes 7 and 8). FFAT peptides alone were not visible on native gels.

Figure 2. Comparison of surface electrostatic characteristics of VAP (1-125) and MSP-1.

(A and B) Two orientations of the VAP (1-125) monomer in surface representation colored to show the electrostatic potential calculated by APBS as implemented in Pymol using the CHARMM force field. The electrostatic surface was contoured from –10 kT/e (red) to +10 kT/e (blue).

(C and D) Two orientations of the MSP-1 dimer equivalent to the VAP (1-125) orientations in (A and B) with one monomer in surface representation and the partner monomer in ribbon representation (orange). The MSP-1 surface is colored to show the electrostatic potential calculated by APBS as implemented in Pymol using the CHARMM force field. The electrostatic surface was contoured from –10 kT/e (red) to +10 kT/e (blue).

Figure 3. ORP1 FFAT motif interaction with the VAP (1-125) FFAT binding site.

(A) The FFAT motif of ORP1 (shown in stick representation) binds across VAP (1-125) (shown in ribbon representation) beta strands F, E, C, and D1. (B) A zoomed view of VAP (1-125) (white carbon atoms) with bound FFAT motif (yellow carbon atoms) is shown in an orientation similar to that in panel A. Electron density for the FFAT motif from a phase-combined σ_A -weighted simulated annealing omit map that omitted FFAT peptide residues from map calculations is shown as blue mesh. ORP1 FFAT residue F476 binds in a cavity bordered by aliphatic side chains that include VAP Lys87 and Met89. (C) The ORP1 FFAT motif binds VAP on a positive surface. The ORP1 FFAT peptide is shown in stick representation. VAP is oriented as in panel A and the surface is colored according to electrostatic potential as in figure 2. (D) The ORP1 FFAT motif binds in a region that is highly conserved among VAP homologues but not in the related protein MSP-1. Residues shown in red are identical among VAP homologues but not conserved in MSP-1 and correspond to those marked with a red star in the alignment in supplemental figure 1B. Residues shown in pink are similar among VAP homologues but are not conserved in MSP-1 and correspond to those marked with a pink triangle in the alignment in supplemental figure 1B. Residues shown in white are conserved in VAP homologues and in MSP-1. Residues shown in grey are not conserved among VAP homologues.

Figure 4. The VAP-FFAT 2:2 complex.

(A and B) The VAP-FFAT complex observed in the crystal structure buries two FFAT motifs (shown in stick representation) between two VAP (1-125) domains (shown in ribbon representation). Panels A and B show the VAP-FFAT complex from two views related by the 90 degree rotation shown. VAP residue Cys53 is colored red to orient the viewer. Panel A illustrates a plausible orientation for the VAP:FFAT complex on membranes. VAP coiled-coil domains (residues 164-192) are shown in dark blue and VAP transmembrane domains (residues 223-241) are shown in light blue. (C) Schematic drawing of interactions between the two FFAT motifs and between VAP and FFAT motifs. This panel shows the same orientation as that in panel B. The background behind VAP molecules is colored to match the VAP chains in panel B. Hydrophobic Van der Waals contacts are indicated by colored bars.

Figure 5. FFAT binding is a major VAP function that is conserved among eukaryotes.

Expression of a mutant of the yeast VAP homologue Scs2p that cannot bind the FFAT motif fails to complement the inositol auxotrophy of an *scs2*Δ yeast strain. (A) Mutant *scs2*Δ strain was transformed with CEN/ARS plasmids expressing *SCS2* or *scs2*-K84D/L86D. The *scs2*Δ strain transformed with the empty vector failed to grow on media lacking inositol. Expression of wildtype Scs2p from the plasmid pSCS2 rescued this growth defect. Expression of the mutant Scs2p K84D/L86D failed to complement the growth phenotype, indicating that this mutant is unable to activate transcription of the INO1 gene. (B) Immunoblot analysis of Scs2p steady state protein levels. Equal amounts of whole cell yeast protein extract were separated by SDS-PAGE and transferred to nitrocellulose. Blots were probed using rabbit anti-Scs2p serum.

Figure 6. Overexpression of full-length VAP or an FFAT-binding mutant causes altered ER morphology.

All bars, 10 μm. **(A)** Full-length VAP-GFP expressed in COS7 cells displays a pattern typical for ER proteins. The boxed area is shown in detail in the righthand panels (calreticulin, VAP-GFP and calreticulin overlay) **(B)** VAP-GFP does not overlay with microtubules. The boxed area is enlarged to show a detailed view of microtubules and VAP-GFP (right panel). **(C)** VAP-GFP overexpression often results in areas of intense fluorescence that are continuous with normal-appearing ER (see inset). **(D)** Intense fluorescent patches colocalize with calreticulin (red, right panel), indicating that they are likely composed of ER membrane. **(E)** A very dense network of ER fills significant areas of the cytoplasm in many cells overexpressing VAP-GFP. The boxed area is shown in detail in the righthand panels (VAP-GFP, calreticulin, overlay). **(F)** These areas of denser ER are more commonly seen in VAP K87D/M89D-GFP-expressing cells. **(G and H)** Unlike wild-type VAP, VAP K87D/M89-GFP localizes in some cells to very regularly-spaced areas of intense fluorescence that are continuous with normal-appearing ER and contain calnexin (red).

Tables

Table 1: VAP (1-125) Se– MAD Crystallographic Data Collection, Phasing, and Refinement Statistics

Crystallographic Data and Phasing
space group $P4_22_12$
cell dimensions a = 48.2 Å, b = 48.2 Å, c = 112.4 Å

		d_{min} (Å)	no. of reflections	complete-ness	< I > / < σ >	R_{sym}[a]	multiplicity
λ1 inflection	(0.9795 Å)	1.7	36231	98.0 (99.8)[b]	16.5 (8.3)	10.1 (42.0)	12.9 (11.9)
λ2 peak	(0.9793 Å)	1.7	36281	98.1 (99.8)[b]	15.5 (7.8)	10.2 (41.0)	12.9 (12.1)
λ3 remote	(0.9649 Å)	1.7	36268	98.0 (99.8)[b]	17.2 (8.1)	9.8 (40.0)	12.9 (11.8)

Observed Dispersive and Bijvoet Ratios[c]

	λ1	λ2	λ3
λ1	0.0585	0.0537	0.0749
λ2		0.1146	0.0637
λ3			0.0724

Se-MAD figure of merit 0.79 (0.70)

Refinement

Resolution range	55-1.7 Å
No. of reflections	27484
R^d	22.1% (27.6%)
R^e_{free}	25.4% (30.0%)
Luzatti coordinate error	0.22 Å
Cross validated Luzatti coordinate error	0.26 Å
Bond-length deviation	0.005 Å
Bond-angle deviation	1.36°
Average B factor	20.5 $Å^2$
Bonded main chain atom B factor rmsd	1.45 $Å^2$
Bonded side chain atom B factor rmsd	2.53 $Å^2$
Residues in the most favored ϕ–ψ region	94.5%
Residues in generously allowed region	5.5%
Residues in disallowed regions	0.0%

[a] $R_{sym} = \Sigma_h\Sigma_i \ |I_i(h)-<I(h)>| \ / \ \Sigma_h\Sigma_i|I_i(h)|$. [b] Values in parentheses are for the highest resolution bin. [c] Values are $<(\Delta|F|)^2>^{1/2}/<|F|^2>^{1/2}$, where Δ|F| is the dispersive (off-diagonal element), or Bijvoet difference (diagonal elements), computed between 500 and 1.7 Å resolution. [d] $R = \Sigma(|F_{obs}|-k|F_{calc}|)/\Sigma|F_{obs}|$. [e] Free R value is the R value obtained for a test set of reflections, consisting of a randomly selected 10% subset of the diffraction data, not used during refinement.

Table 2: VAP-FFAT complex – Crystallographic Data Collection, Phasing, and Refinement Statistics

Crystallographic Data and Phasing
space group P1
cell dimensions a = 50.1 Å, b = 50.0 Å, c = 90.3 Å, $\alpha = 90^{o}$, $\beta = 90^{o}$, $\gamma = 60^{o}$

		d_{min} (Å)	no. of reflections	complete-ness	< I > / < σ >	R_{sym} [a]	multiplicity
Se-SAD	(0.9794 Å)	2.8	119160	99.0 (99.9)[b]	14.4 (9.4)	9.3 (21.0)	7.9 (7.8)
Native	(1.0331 Å)	1.9	59506	99.4 (100.0)[b]	10.2 (3.8)	6.0 (34.0)	4.0 (4.0)

Se-SAD FOM 0.38 (0.34)
Se-SAD FOMDM 0.84 (0.79)

Refinement

Resolution range	14.65-1.9 Å
No. of reflections	53477
R^{c}	22.5% (28.0%)
R^{d}_{free}	25.7% (32.1%)
Luzatti coordinate error	0.21 Å
Cross validated Luzatti coordinate error	0.17 Å
Bond-length deviation	0.034 Å
Bond-angle deviation	2.71^{o}
Average B factor	33.1 $Å^{2}$
Bonded main chain atom B factor rmsd	1.54 $Å^{2}$
Bonded side chain atom B factor rmsd	2.86 $Å^{2}$
Average NCS rmsd (all atoms)	0.03 Å
Residues in the most favored ϕ–ψ region	93.8%
Residues in generously allowed region	6.2%
Residues in disallowed regions	0.0%

[a] $R_{sym} = \Sigma_h \Sigma_i |I_i(h) - \langle I(h) \rangle| / \Sigma_h \Sigma_i |I_i(h)|$. [b] Values in parentheses are for the highest resolution bin. [c] $R = \Sigma(|F_{obs}| - k|F_{calc}|)/\Sigma|F_{obs}|$. [d] Free R value is the R value obtained for a test set of reflections, consisting of a randomly selected 10% subset of the diffraction data, not used during refinement.

[Insert Running heads here]

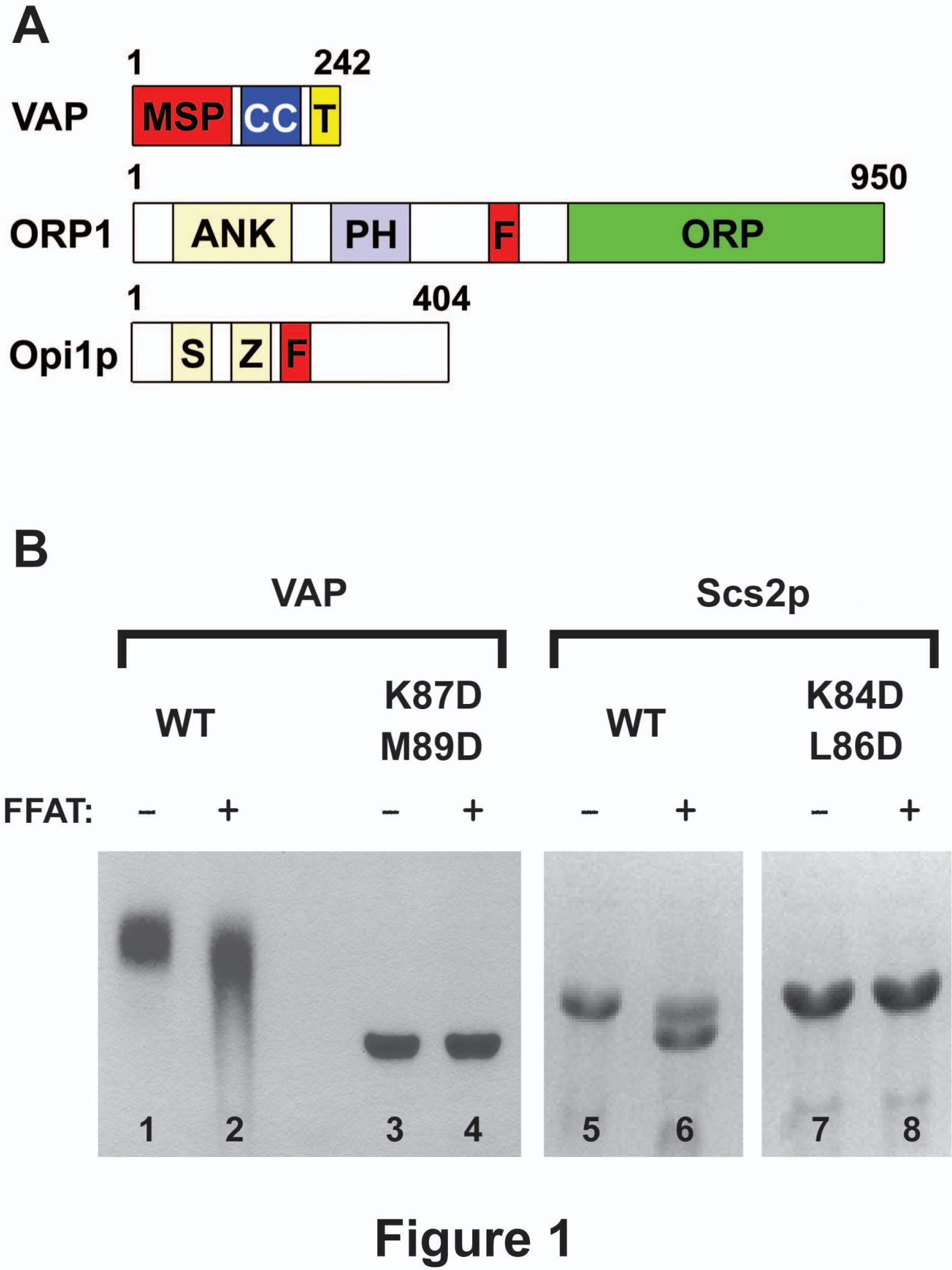
A
1
242
VAP
MSP
CC
T
1
950
ORP1
ANK
PH
F
ORP
1
404
Opi1p
S
Z
F
B
VAP
Scs2p
WT
K87D
M89D
WT
K84D
L86D
FFAT:
–
+
–
+
–
+
–
+
1
2
3
4
5
6
7
8

Figure 1

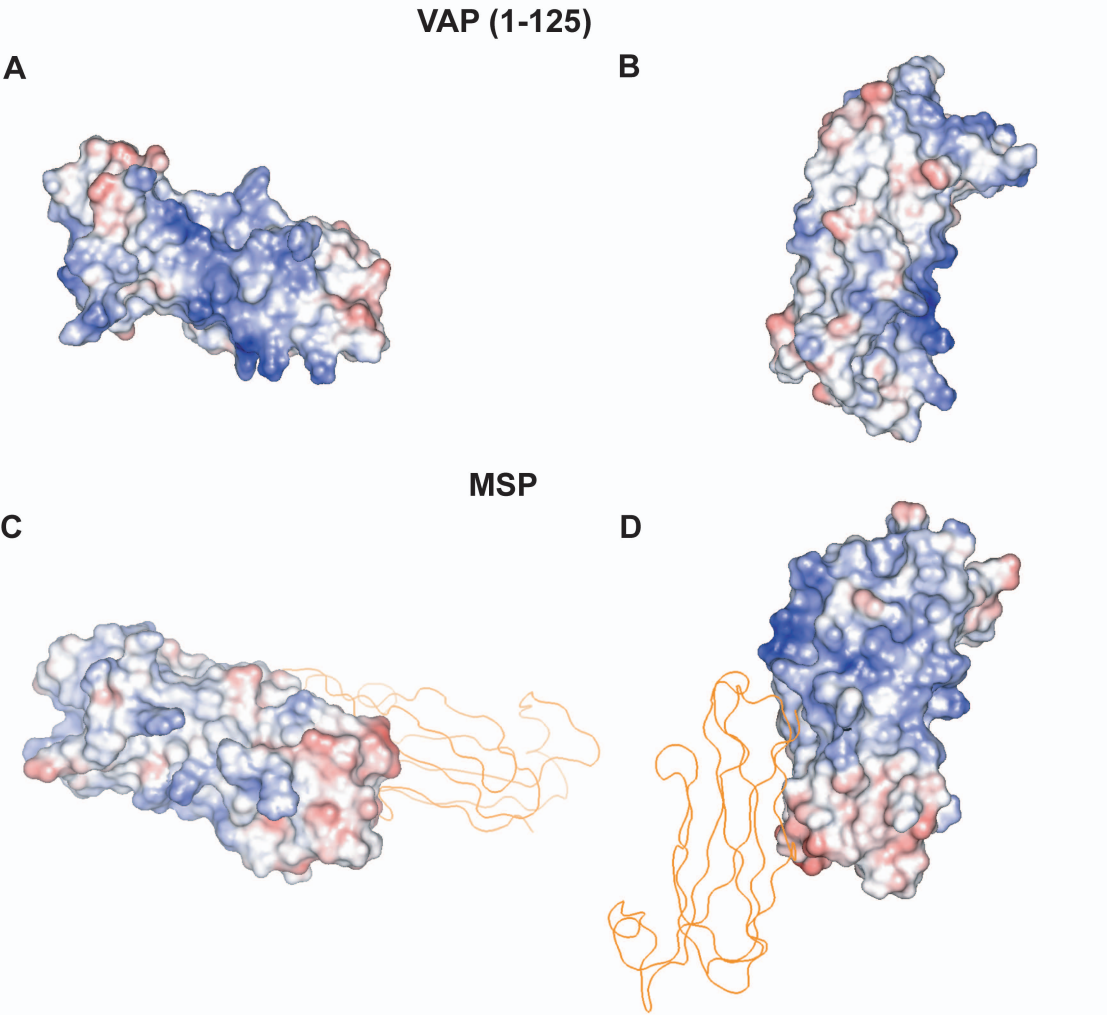

Figure 2

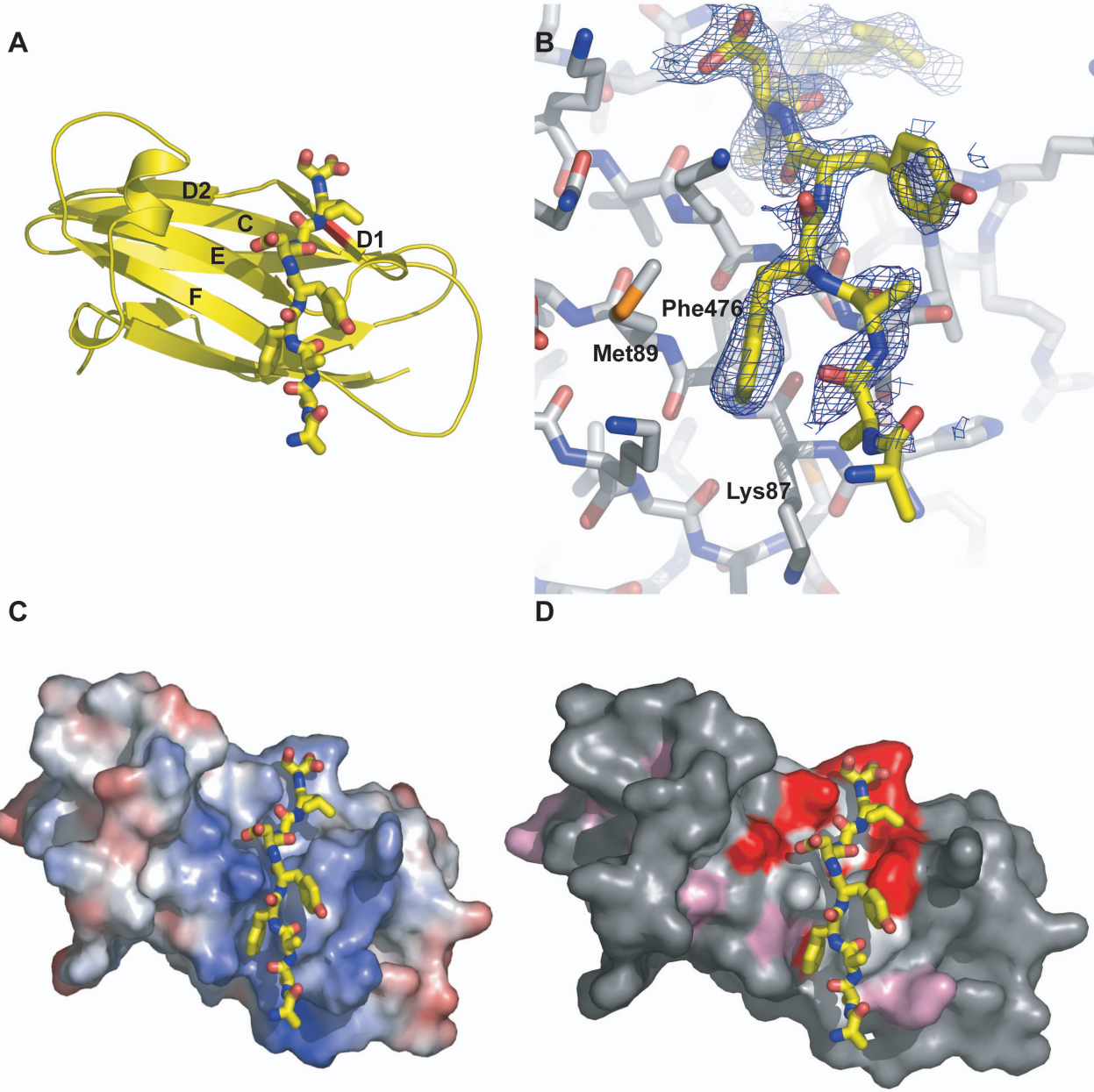

Figure 3

Figure 4

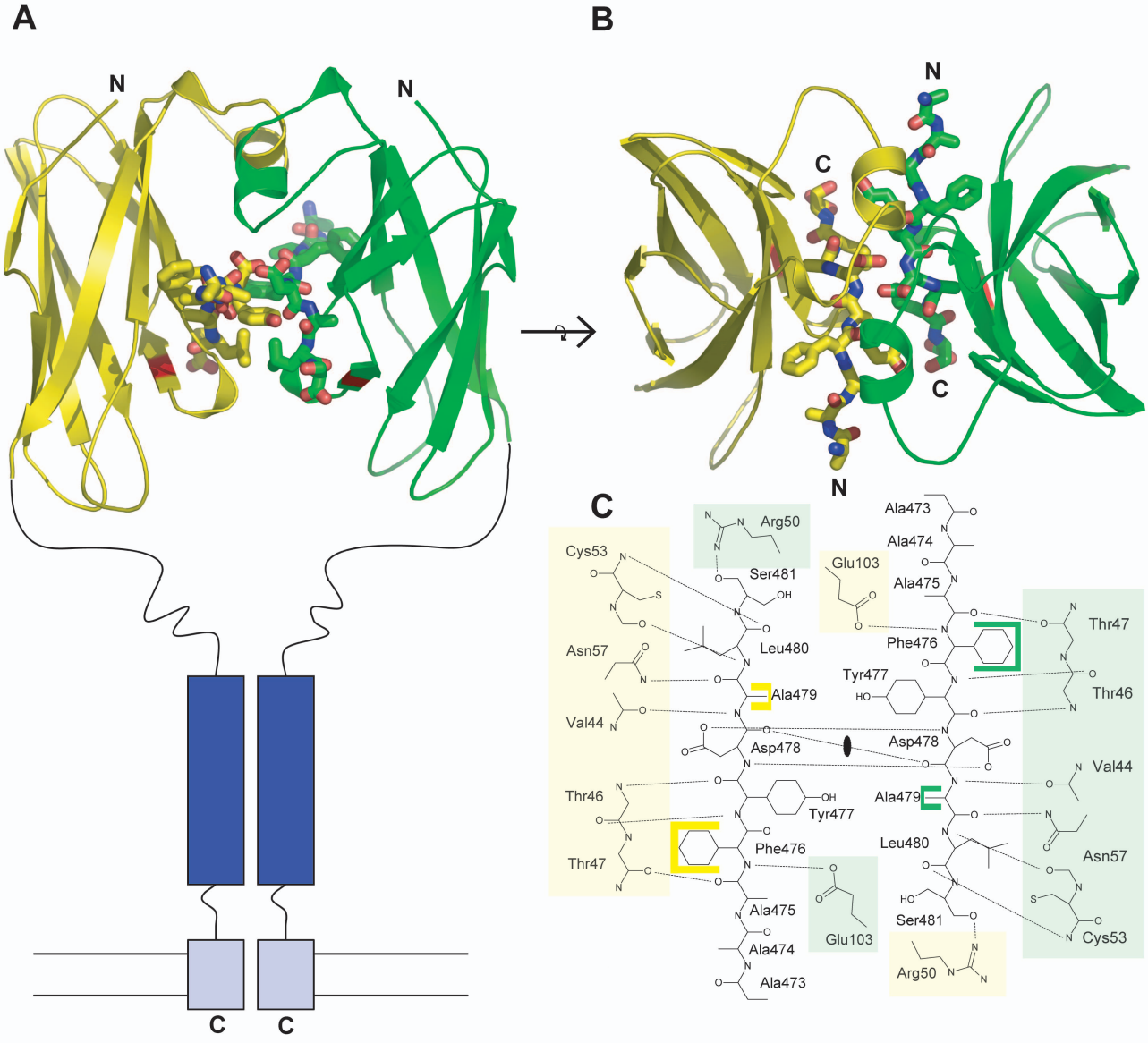
A
B
C
N
N
C
C
N
C
C
Arg50
Cys53
Ser481
Glu103
Ala473
Ala474
Ala475
Thr47
Phe476
Asn57
Leu480
Tyr477
Thr46
Ala479
Val44
Asp478
Asp478
Val44
Thr46
Ala479
OH
Tyr477
Leu480
Asn57
Phe476
Thr47
Ala475
Glu103
Ser481
Ala474
Cys53
Ala473
Arg50

Figure 5

A

plasmid

SCS2

scs2Δ

-

WT

K84D/L86D

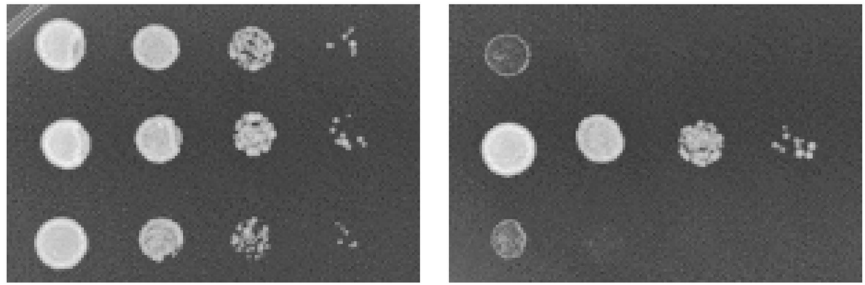

B

Strain: SCS2 scs2Δ

plasmid: - vector pSCS2 pscs2-K84D/L86D

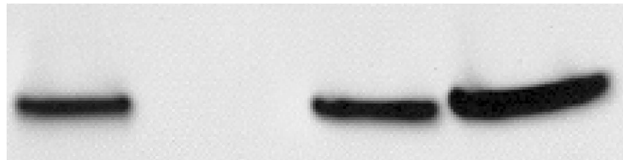

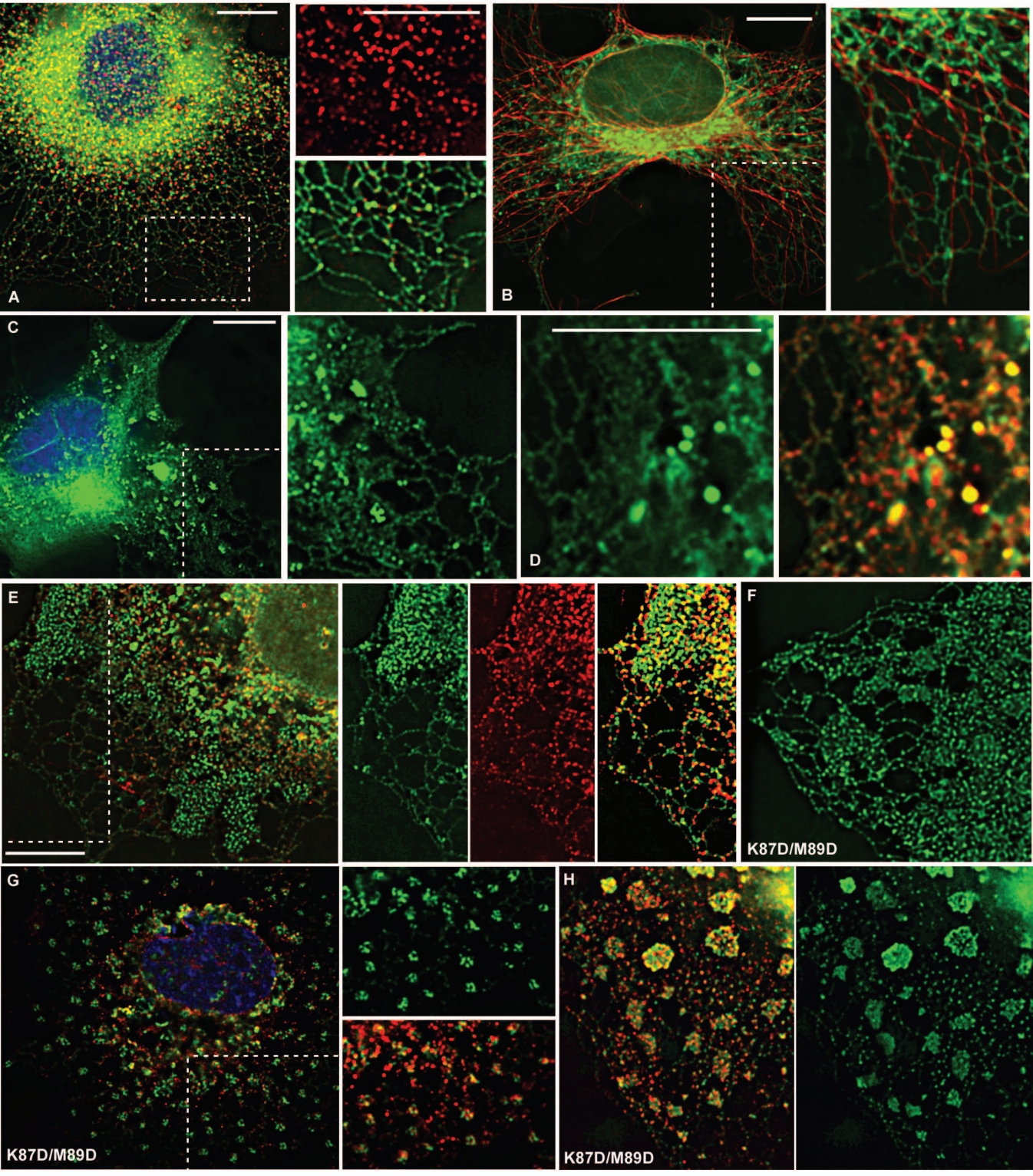

Figure 6

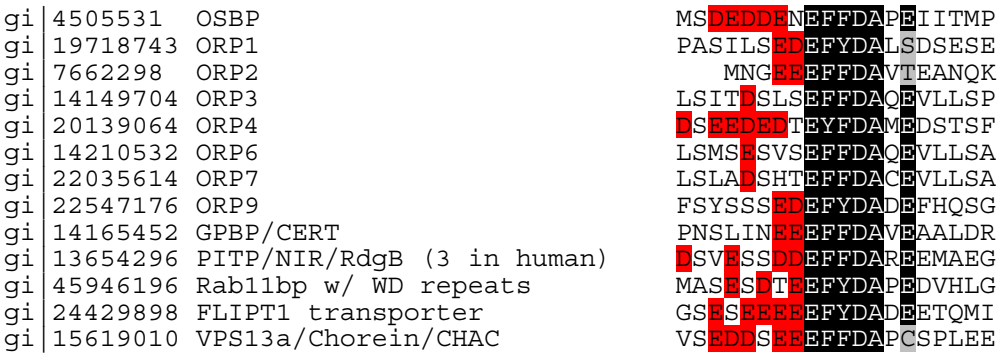

Supplemental Figure 1A. Alignment of human proteins containing putative FFAT motifs selected from those found by a MEME/MAST search (http://meme.sdsc.edu/). A wide variety of proteins contain sequences that approximate the FFAT motif as initially defined (Loewen et al., 2003) and the motif still requires more precise definition. Those shown here are not predicted to reside in beta sheet secondary structure.

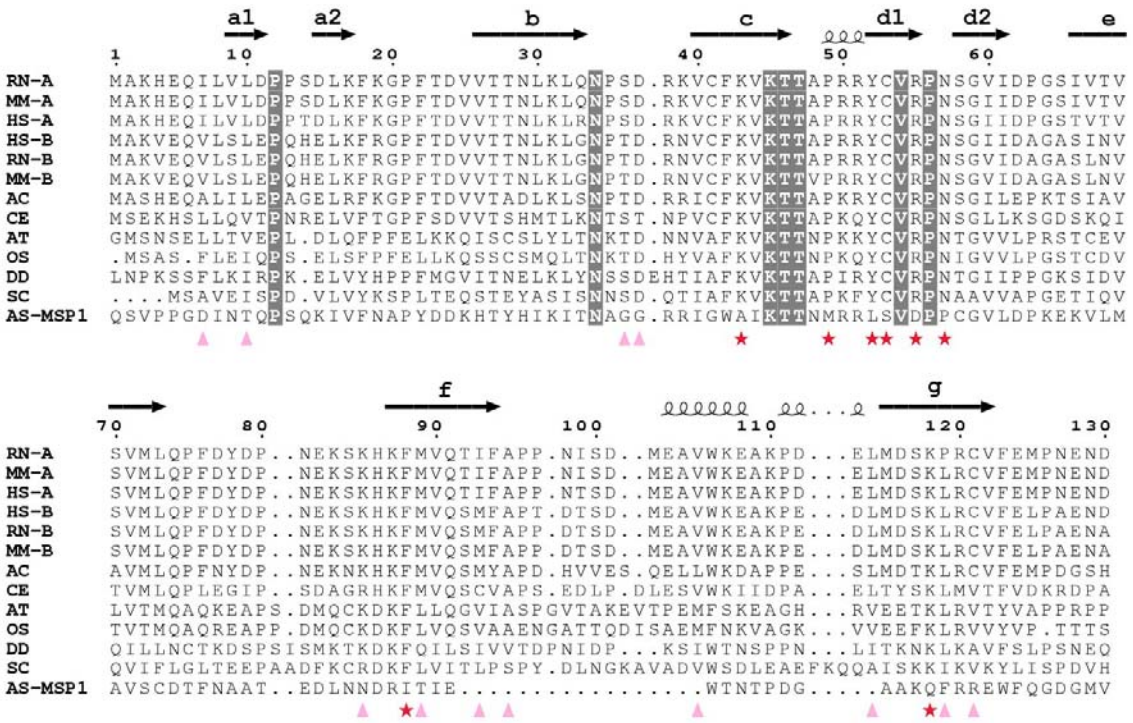

Supplemental Figure 1B. Alignment of the MSP homology domain that is highly conserved among all VAP protein family members. Family members were selected from a broad variety of eukaryotes, including: VAP proteins from Rattus norvegicus (RN); Homo sapiens (HS); Mouse musculus (MM); Aplysia californica (AC); Caenorhabditis elegans (CE); Arabidopsis thaliana (AT); Oryza sativa (OS); Dictyostelium discoidum (DD); Saccharomyces cerevisiae (SC). For comparison, Ascaris suum Major Sperm Protein 1 is the last sequence in the alignment. The seven beta strands (a-g) that constitute this domain are represented above rat VAP-A. Residues that are identical in all VAP proteins and in MSP-1 are shaded grey. Residues that are identical among VAP homologues, but are not conserved in MSP-1 are marked with red stars. Residues that are highly conserved among VAP homologues, but not in MSP-1, are marked with pink triangles.

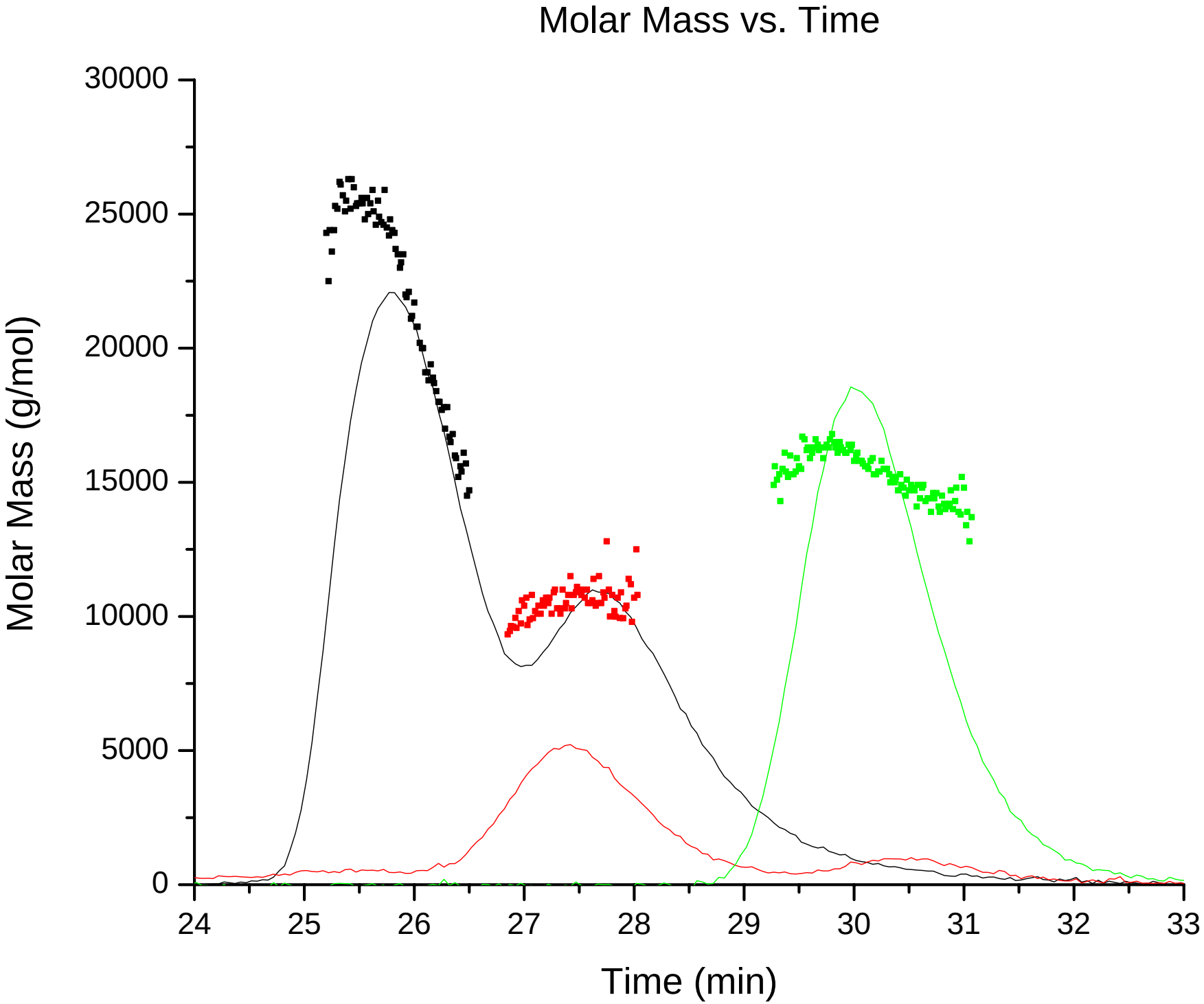
Molar Mass vs. Time
Molar Mass (g/mol)
30000
25000
20000
15000
10000
5000
0
24
25
26
27
28
29
30
31
32
33
Time (min)


Time (min):
24
24.5
25
25.5
26
MW
26.5
27
27.5
28
28.5
29
VAP
FFAT

Supplemental Figure 2. Analysis of VAP-FFAT complex solution behavior by Size-Exclusion Chromatograhy (Superdex 75) coupled to in-line Multi-Angle Laser Light Scattering (SEC-MALLS) (DAWN EOS system, Wyatt Technology) with in-line refractive index detection. A value of 0.185 ml/g was assumed for the dn/dc of the protein. Peaks (solid lines) are relative light scattering at 90 degrees with molar mass of the species superimposed (dotted lines) in the same color. VAP (1-125) loaded at 0.6 mM (green) elutes as monomer with MW ~15 kD. ORP1 (454-546) loaded at 0.6 mM (red) elutes as monomer with MW ~10 kD. When both VAP (1-125) and ORP1 (454-546) are loaded at 0.6 mM each (black), a peak elutes at 26 minutes containing a species consistent with a 1:1 VAP-FFAT complex with MW ~25 kD; the decrease of the molar mass at longer elution times indicates partial dissociation of the complex. For the VAP-FFAT experiment, SDS gels were run with fractionated SEC-MALLS eluant. VAP was present in fractions that eluted from 24.5-29 minutes. ORP1 (454-546) eluted at an approximately equimolar ratio with VAP from 24.5-26 minutes and was present in decreasing amounts at longer elution times. This behavior is consistent with partial dissociation of the complex due to the approximately 1 μM affinity previously measured for VAP-FFAT interactions (Loewen et al., 2003). The peak at 27.5 minutes in the VAP-FFAT experiment contains primarily VAP (1-125) and likely results from dissociation of the VAP-FFAT complex. SEC-MALLS experiments with VAP (1-125) and the FFAT peptide crystallized in this study are also consistent with 1:1 stoichiometry (data not shown).